Charge Transport in DNA Duplex/Quadruplex Conjugates†

Sarah Delaney and Jacqueline K. Barton*

Division of Chemistry and Chemical Engineering, California Institute of Technology, Pasadena, California 91125

Received July 8, 2003; Revised Manuscript Received September 12, 2003

ABSTRACT: DNA conjugates containing adjacent duplex and guanine quadruplex assemblies have been designed to explore charge transport into quadruplex architectures. The quadruplex assemblies have been characterized structurally using circular dichroism and by assaying for chemical protection. Using an intercalating rhodium photooxidant, noncovalently bound or tethered to the duplex end, oxidizing radicals are found to be trapped in the folded quadruplex. Damage is observed almost exclusively at the external tetrads of the quadruplex. Little damage of the center tetrad is observed, due most likely to lowered efficiency of radical trapping within the quadruplex core. This pattern of damage is distinct from that observed for repetitive G sequences within duplex DNA. The data indicate, furthermore, that in the conjugates examined, the guanine quadruplex provides a more effective trap than a 5′-GG-3′ guanine doublet within duplex DNA. Within these assemblies, sufficient base−base overlap must exist at the duplex/quadruplex junction to allow for charge migration. This funneling of damage to the quadruplex, as well as the unique pattern of damage within the quadruplex, requires consideration with respect to the analysis of oxidative DNA damage within the cell.

DNA quadruplexes have received a wealth of attention in the recent literature (*1*−*4*). These structures have gained notoriety as inhibitors of telomerase (*5*), the enzyme that provides cancerous cells immortality, and quadruplex formation has recently been implicated as a transcriptional repressor element (*6*). The unique structure of guanine quadruplexes consists of stacked tetrads where each tetrad, as shown in Figure 1, is a planar array of four Hoogsteen-bonded guanines (*7*). The formation of guanine quadruplexes is stabilized by the presence of monovalent cations (e.g., K^+, Na^+) positioned in the center of the structure and coordinated by the electron-rich carbonyl oxygens (*8*, *9*). Quadruplexes can form in an intramolecular fashion from a single strand, from two DNA hairpins, or from four individual strands. Depending on the strand orientation, both parallel and antiparallel quadruplexes are possible (*10*).

DNA quadruplexes have been proposed to form at telomeres (*7*, *11*), the repetitive DNA sequence located at the ends of linear chromosomes. Human telomeric DNA is composed of approximately 10 kb of double stranded (5′-TTAGGG-3′)$_n$ repeats (*12*). The extreme 3′-end is a 200−300 base single stranded overhang of the guanine containing strand (*13*). These guanine-rich single stranded overhangs have been shown in vitro to form guanine quadruplexes (*10*). Of particular relevance to the studies described here, it has been proposed that these guanine-rich telomeric regions may serve as hot spots for oxidative DNA damage within the genome (*14*).

Oxidative damage to DNA has been shown to arise not only as a result of reaction of DNA with an impinging oxidant but also as a result of reaction from a distance through DNA charge transport (CT)[1] from a remotely bound oxidant (*15*−*18*). The base stack of B-DNA has been shown to mediate CT over a distance of 200 Å (*19*, *20*). By triplex targeting of a photooxidant to long DNA restriction fragments, the typical distance regime for long-range oxidative damage to DNA by CT was shown to be ∼ 60 bp (*21*). DNA packaged within a nucleosome core particle is also subject to oxidative damage from a distance (*22*). Moreover, long-range oxidative damage to DNA has been demonstrated within *Hela* cell nuclei (*23*). Thus, oxidative damage to DNA from a distance through DNA CT chemistry provides a feasible mechanism for the generation of cellular base lesions and now requires consideration as a mechanism for DNA damage within the cell.

In that context, it has been suggested that telomeric regions of DNA, rich in guanine-containing repetitive sequences and hot spots for oxidative damage, might provide regions to which oxidizing equivalents are funneled through long-range CT. Heller has proposed a means of cathodic DNA protection similar to the way in which Zn^{2+} protects steel (*24*). The number of 5′-GGG-3′ triple guanine sites was shown statistically to be elevated in the regions flanking protein-coding exons; thus, it was suggested that charges injected into DNA might be funneled to these sacrificial guanine-rich introns or to the nonprotein coding sequences of guanine-rich telomeric DNA. Our studies of the distance regime for long-range oxidative damage indicate that funneling of all damage to telomeres is unlikely, and electrochemical studies of oxidative damage in quadruplexes have suggested that the structure is not more reactive to accessible oxidants than duplex DNA (*25*). It is of interest, nonetheless, to establish whether telomeric regions and the quadruplex structures proposed to form within telomeres might represent domains

† This work was supported by NIH.

* To whom correspondence should be addressed. E-mail: jkbarton@caltech.edu.

[1] Abbreviations: CT, charge transport; DMS, dimethyl sulfate.

10.1021/bi0351965 CCC: $25.00
Published on Web 11/13/2003

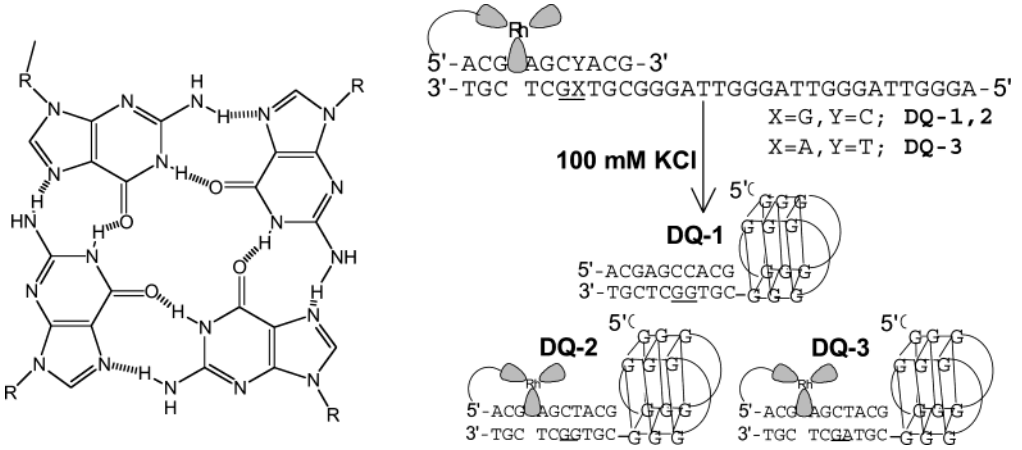

FIGURE 1: Schematic illustrations of a guanine tetrad (left) and the duplex/quadruplex conjugates **DQ-1**, **DQ-2**, and **DQ-3** (right) utilized in this paper (adenines and thymines have been schematized for clarity). In the presence of 100 mM KCl, the single stranded overhang folds intramolecularly into an antiparallel quadruplex.

for long-range CT. Here, we describe long-range CT to quadruplex structures to effect oxidative DNA damage.

MATERIALS AND METHODS

Oligonucleotide Synthesis and Formation of DNA Duplex/Quadruplex Conjugates. Oligonucleotides were synthesized on an ABI 392 DNA/RNA synthesizer, using standard phosphoramidite chemistry (*26*). DNA was purified by HPLC using a Dynamax 300 Å C18 reverse-phase column (Rainin) (100% 30 mM NH_4OAc to 85% 30 mM NH_4OAc/15% acetonitrile over 30 min). Quantification was done on a Beckman DU 7400 spectrophotometer using the ϵ_{260} values estimated for single stranded DNA (*27*). The $[Rh(phi)_2bpy']^{3+}$ (phi = phenanthrenequinone diimine, bpy′ = 4′-methylbipyridine-4-butyric acid) tethered oligonucleotides were prepared as described previously (*28*) and were purified by HPLC on a Dynamax 300 Å C18 reverse-phase column (85% 30 mM NH_4OAc/15% acetonitrile to 75% 30 mM NH_4OAc/25% acetonitrile over 40 min). The rhodium-conjugated oligonucleotides were characterized by mass spectrometry (MALDI) and quantitated by UV−vis using an extinction coefficient of $\epsilon_{350} = 23\,600\ M^{-1}\ cm^{-1}$. To form the DNA duplex/quadruplex conjugate, equimolar concentrations of the quadruplex forming strand and the 10 base complement were annealed in 10 mM potassium phosphate, pH 7 with 100 mM KCl. Samples were heated to 90 °C and slowly cooled to room temperature.

Circular Dichroism Measurements. CD spectra were obtained on an AVIV CD spectrometer at room temperature. Unmetalated oligonucleotides were utilized for all CD measurements to avoid a signal from the rhodium photooxidant. The conjugate concentration was 2.5 μM, duplex was 4 μM, and quadruplex forming strand alone was 4 μM, and all were in 10 mM potassium phosphate, pH 7 with 100 mM KCl. The melting profile of the conjugate (2.5 μM) was obtained by slowly lowering the temperature (0.5 °C/min) from 85 to 25 °C and monitoring the ellipticity at 285 nm. The melting temperature value represents the midpoint of the transition as obtained by fitting the melting profile with a sigmoidal expression.

Dimethyl Sulfate Protection Assay. The quadruplex forming single strand was 5′-^{32}P end-labeled using standard protocols, and the conjugate was annealed at a concentration of 4 μM. The duplex control was also annealed at a concentration of 4 μM. The assemblies were treated with 10% (v/v) DMS for 10 min at ambient temperature; reactions were stopped by adding quenching buffer (1 M β-mercaptoethanol, 1.5 M sodium acetate, pH 7). Samples were ethanol precipitated and treated with 10% piperidine (v/v) at 90 °C for 30 min, dried, and electrophoresed through a 20% denaturing polyacrylamide gel. The extent of methylation was visualized by phosphorimagery (ImageQuant).

Native Gel Electrophoresis. The quadruplex forming single strand was 5′-^{32}P end-labeled using standard protocols, and the conjugate was annealed at a concentration of 4 μM in 10 mM potassium phosphate, pH 7 with 100 mM KCl. Samples were electrophoresed at 4 °C and 10 W for ~12 h through a 12% nondenaturing gel containing 100 mM KCl in the gel matrix, running buffer (0.5X TBE), and loading dye. The products were visualized by phosphorimagery (ImageQuant).

Assay of Oxidative DNA Damage. The quadruplex forming single strand was 5′-^{32}P end-labeled as stated previously, and the conjugates were annealed at a concentration of 4 μM. Experiments utilizing noncovalently bound photooxidant contained 4 μM $[Rh(phi)_2bpy']^{3+}$. For the rhodium photocleavage experiments, samples were irradiated at 313 nm with a 1000 W Hg/Xe lamp equipped with a monochromator and dried following irradiation. For the CT experiments, samples were irradiated at 365 nm, treated with 10% (v/v) piperidine at 90 °C for 30 min, and dried, and all samples were electrophoresed through a 20% denaturing polyacrylamide gel. The extent of damage was visualized by phosphorimagery (ImageQuant).

RESULTS

Design of Duplex/Quadruplex Assemblies. DNA conjugates containing adjacent duplex and guanine quadruplex structures were designed as shown in Figure 1. First, we examined oxidative damage in a duplex/quadruplex conjugate (**DQ-1**) using noncovalently bound $[Rh(phi)_2bpy']^{3+}$. The rhodium photooxidant is particularly useful owing to its well-characterized photochemistry with DNA. Upon high energy irradiation (λ = 313 nm), this rhodium complex promotes direct strand cleavage owing to hydrogen atom abstraction from the sugar ring closest to the intercalation site; this

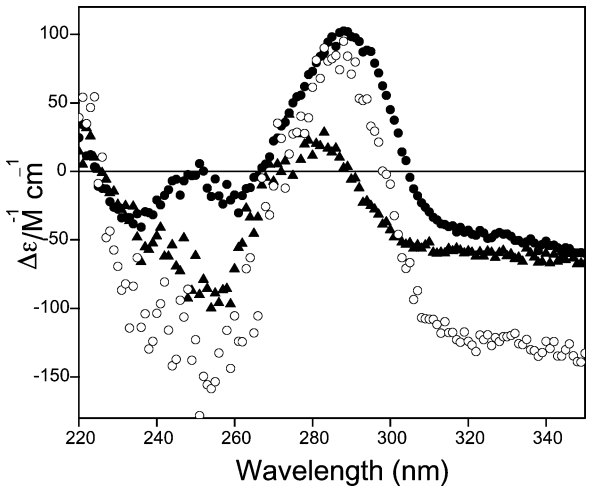

FIGURE 2: CD spectra of the quadruplex forming strand alone of **DQ-1** (closed circles), 10 base pair duplex of **DQ-1** alone (closed triangles), and **DQ-1** (open circles). The spectra were obtained at ambient temperature in 10 mM potassium phosphate, pH 7 with 100 mM KCl and at concentrations of 4 μM for the quadruplex forming strand alone and duplex and 2.5 μM for **DQ-1**.

reaction marks the site of binding by the photooxidant (*29*). When irradiated at lower energy ($\lambda = 365$ nm), the rhodium complex promotes guanine oxidation at sites remote from the photooxidant via DNA CT (*30*); with piperidine treatment, irreversible oxidative damage is revealed.

In designing **DQ-1**, a 10 base pair duplex region was selected to provide a suitable binding site for the photooxidant and to contain a 5′-GG-3′ guanine doublet, while the 22 bases of the single stranded overhang should form an intramolecular guanine quadruplex. A crystal structure of this 22 base single strand in the presence of K^+ indicates formation of a parallel quadruplex (*31*), while an NMR solution structure in the presence of Na^+ indicates formation of an antiparallel quadruplex (*32*). Circular dichroism studies show formation of an antiparallel quadruplex in the presence of either K^+ or Na^+ (*33*).

An assembly analogous to **DQ-1** contains the rhodium photooxidant covalently tethered to the end of the duplex (**DQ-2**). In a third assembly, **DQ-3**, which also includes a covalently tethered rhodium photooxidant, a single base pair has been changed to yield a 5′-GA-3′ in the duplex region. These three conjugates allow us to probe CT between the two distinct regions, duplex and quadruplex. Additionally, in the conjugates containing a covalently bound rhodium photooxidant, CT through duplex/quadruplex junctions can be examined.

Characterization of DNA Duplex/Quadruplex Conjugates by Circular Dichroism. Antiparallel and parallel guanine quadruplexes possess characteristic and distinct circular dichroism spectra. Antiparallel quadruplexes are characterized by maxima at 290 nm and minima at 260 nm; parallel quadruplexes possess maxima at 260 nm and minima at 240 nm (*34*, *35*). To fully characterize a single DNA conjugate by CD, three assemblies were examined; the first contains only the quadruplex forming strand with no 10 base complement; the second assembly consists of the 10 base pair duplex with no 22 base overhang; and the third assembly is the duplex/quadruplex conjugate. Figure 2 shows the circular dichroism spectra for the quadruplex forming strand alone of **DQ-1** (closed circles), 10 base pair duplex of **DQ-1** alone (closed triangles), and **DQ-1** (open circles). For the quadruplex forming strand, a maximum at 290 nm in addition to a minimum at 260 nm is observed indicating the formation of an antiparallel quadruplex. The minimum at 240 nm likely results from the 10 bases not involved in quadruplex formation, as this minimum is present even at denaturing temperatures (data not shown). The CD spectrum of **DQ-1** has a maximum at 290 nm indicative of antiparallel quadruplex formation, in addition to a broad minimum centered around 250 nm, similar to that of the 10 base pair duplex alone.

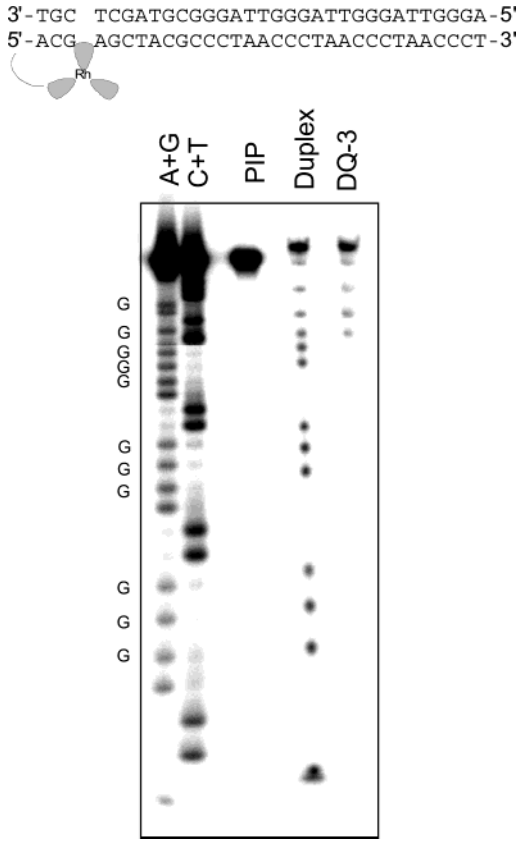

FIGURE 3: DMS methylation protection analysis of **DQ-3** and an all duplex control (sequence shown above). Maxam−Gilbert sequencing reactions A + G and C + T are shown in lanes 1 and 2, respectively. Damage of **DQ-3** treated with piperidine, but not DMS, is shown in lane 3. Lanes 4 and 5 show the methylation of the 32 base pair duplex control and **DQ-3**, respectively. The duplex and conjugate concentrations were 4 μM in 10 mM potassium phosphate, pH 7 with 100 mM KCl.

Protection from Dimethyl Sulfate to Determine Guanine Quadruplex Formation. In double helical DNA, the N-7 of guanine is susceptible to methylation by DMS. However, as seen in Figure 1, the N-7 of guanine in a tetrad is involved in hydrogen bonding and is therefore protected from methylation. Methylation by DMS was examined in the duplex/quadruplex conjugates in addition to control assemblies in which the quadruplex forming strand was base paired to its complement, resulting in a 32 base pair duplex. As seen in Figure 3 for the **DQ-3** duplex control, all guanines in the duplex are methylated, as expected. However, in **DQ-3**, methylation is only observed in the 10 base pair duplex (the first guanine proximal to the duplex, although involved in quadruplex formation, may be transiently accessible by DMS as methylation is observed). The remaining guanines are protected from methylation, consistent with guanine qua-

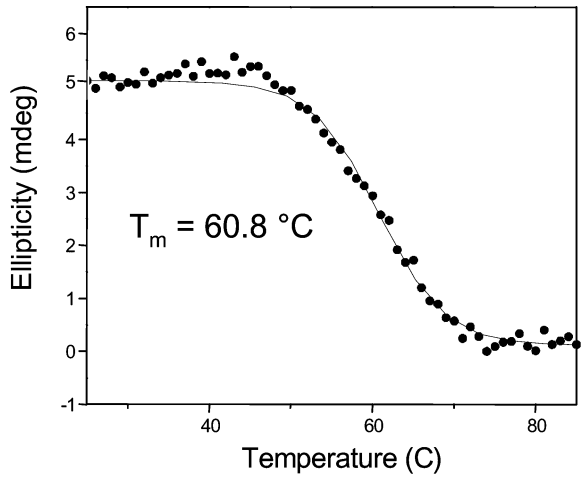

FIGURE 4: CD melting temperature profile of **DQ-1** (2.5 μM), monitored at 285 nm, in 10 mM potassium phosphate, pH 7 with 100 mM KCl. The melting temperature value of 60.8 °C represents the midpoint of the transition obtained by fitting the melting profile to a sigmoidal curve.

druplex formation. Similar methylation patterns were obtained for **DQ-1** and **DQ-2** (Supporting Information).

Structural Analysis by Native Gel Electrophoresis. After electrophoresis through a nondenaturing gel, all three duplex/quadruplex conjugates **DQ-1**, **DQ-2**, and **DQ-3** migrate as single bands, representing a unique structure containing an intramolecular guanine quadruplex (Supporting Information). The observance of only one band indicates the presence of a single species, not multiple species or species containing more than one global conformation. Importantly, since slower moving bands are not observed, the conjugates do not aggregate under the conditions used for the CT experiments.

Melting Temperature Studies of the Duplex/Quadruplex Conjugates. The melting temperature profile of **DQ-1**, monitored at 285 nm by CD, is shown in Figure 4. A single transition is observed. These data were fit to a sigmoidal curve, and the inflection point yields a melting temperature of 60.8 °C for **DQ-1**. Previous studies of this quadruplex forming sequence, performed under comparable salt conditions, revealed little hysteresis between the annealing and the melting curves (*36*). Importantly, the melting temperature is found to be independent of concentration consistent with an intramolecular quadruplex (*36*). Melting temperature experiments were performed for the 10 base pair duplex and quadruplex forming strand alone yielding melting temperatures of 58.6 and 59.0 °C, respectively (Supporting Information). Because of the similarities in melting temperatures, it is not surprising that only one melting transition is observed for **DQ-1**. In fact, the temperature range over which the transition occurs is the same for the quadruplex forming strand alone as for the duplex/quadruplex conjugate.

Charge Transport Chemistry in DNA Duplex/Quadruplex Conjugates. Figure 5 shows the denaturing PAGE of **DQ-1** after photoactivation of the noncovalently bound rhodium intercalator. In the 313 lane, where direct strand cleavage by the rhodium complex is assayed, damage is observed exclusively in the duplex portion of the conjugate, particularly, the two bases adjacent to the quadruplex. These sites may be more accessible to rhodium binding due to the proximity of the quadruplex or duplex fraying. Since the rhodium photooxidant cannot promote direct strand scission

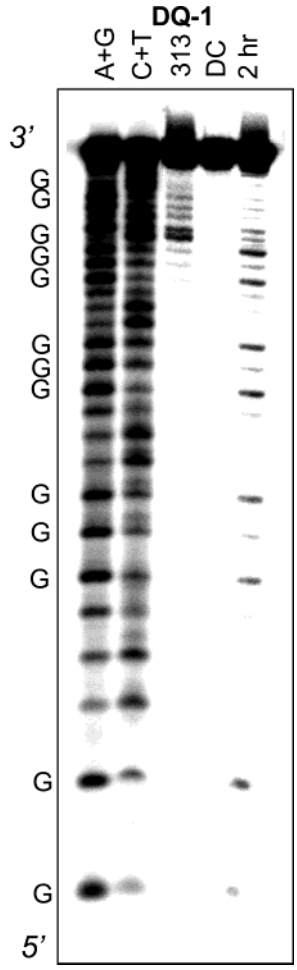

FIGURE 5: PAGE of **DQ-1** after photoactivation of noncovalently bound $[Rh(phi)_2bpy']^{3+}$. Maxam−Gilbert sequencing reactions A + G and C + T are shown in lanes 1 and 2, respectively. Lane 3 shows the direct photocleavage by the rhodium intercalator after irradiation at 313 nm for 30 min. Lanes 4 and 5 display the oxidative damage after irradiation at 365 nm for 0 and 120 min, respectively. Conjugate and noncovalent rhodium photooxidant concentrations were 4 μM in 10 mM potassium phosphate, pH 7 with 100 mM KCl.

on single stranded DNA, the damage observed after irradiation at 313 nm provides evidence that the 10 base pair duplex is indeed forming. Interestingly, with irradiation at 313 nm, no damage is observed in the quadruplex portion of the conjugate. It is noteworthy that when present in excess, this rhodium photooxidant can promote direct strand cleavage within the quadruplex region (data not shown). At equimolar concentrations, however, the oxidant appears to bind preferentially to the duplex rather than quadruplex DNA. Upon irradiation of **DQ-1** at 365 nm in the presence of rhodium photooxidant, damage is observed only in the quadruplex region. Specifically, damage is observed almost exclusively at the 5′-G and 3′-G of each 5′-GGG-3′ guanine triplet comprising the quadruplex. There is very little damage detected at the center Gs of the triplets or within the duplex region.

To explore CT in duplex/quadruplex conjugates where the location of photooxidant binding, and therefore, radical injection are defined, **DQ-2** and **DQ-3** containing the duplex-tethered rhodium intercalator were utilized. Figure 6A shows the denaturing PAGE of both **DQ-2** and **DQ-3** after photoactivation of the rhodium intercalator. In the 313 lanes,

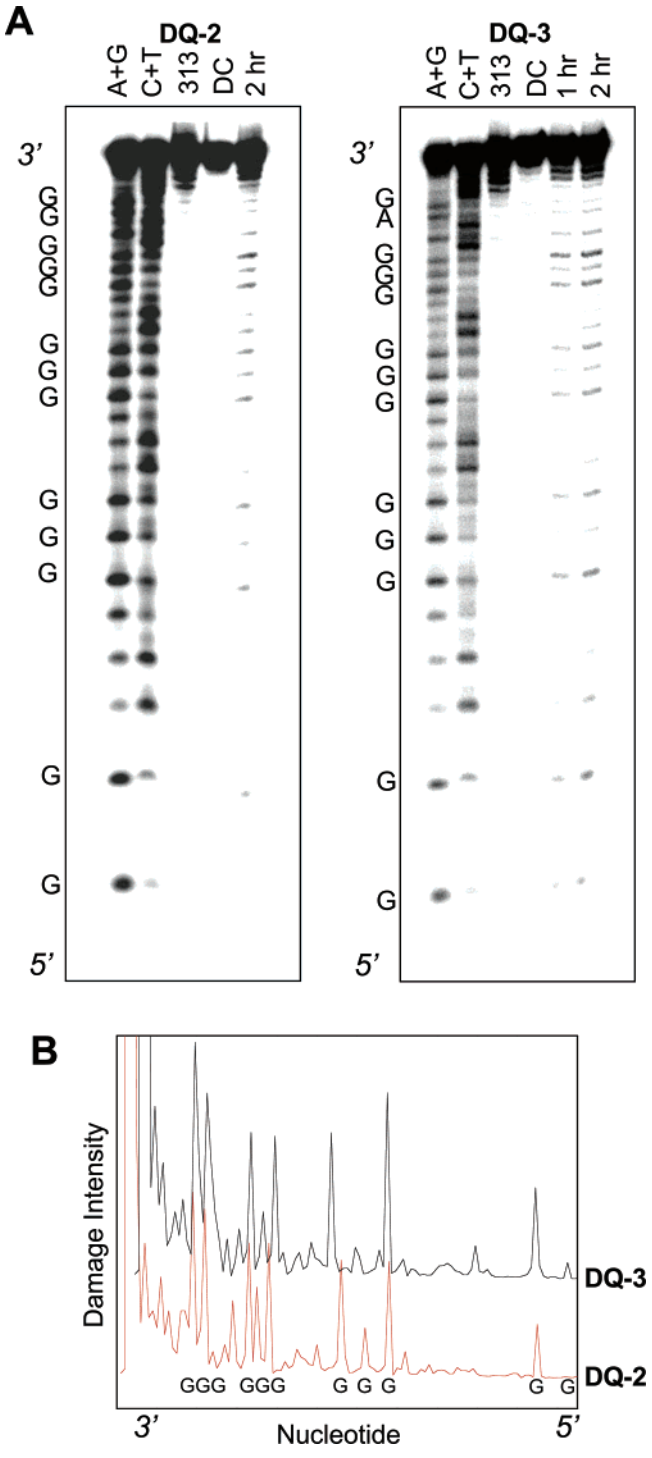

FIGURE 6: (A) PAGE of **DQ-2** and **DQ-3** after photoactivation of covalently tethered $[Rh(phi)_2bpy']^{3+}$. On the left for **DQ-2**, Maxam−Gilbert sequencing reactions A + G and C + T are shown in lanes 1 and 2, respectively. Lane 3 shows the photocleavage of the rhodium intercalator after irradiation at 313 nm for 30 min. Lanes 4−6 display the oxidative damage after irradiation at 365 nm for 0, 60, and 120 min, respectively. On the right for **DQ-3**, Maxam−Gilbert sequencing reactions A + G and C + T are shown in lanes 1 and 2, respectively. Lane 3 shows the photocleavage of the rhodium intercalator after irradiation at 313 nm for 30 min. Lanes 4 and 5 display the oxidative damage after irradiation at 365 nm for 0 and 120 min, respectively. Conjugate concentration was 4 μM in 10 mM potassium phosphate, pH 7 with 100 mM KCl. (B) Histograms of the oxidative damage observed after 120 min of 365 nm irradiation for **DQ-2** (red) and **DQ-3** (black). The plots have been aligned horizontally to allow for direct comparison.

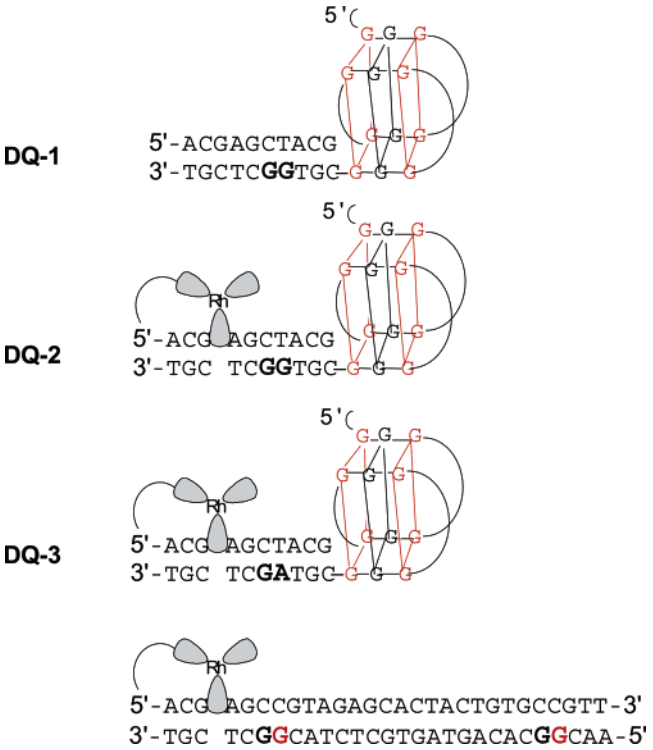

FIGURE 7: Schematic illustrations of the oxidative damage patterns in **DQ-1**, **DQ-2**, and **DQ-3** after CT from $[Rh(phi)_2bpy']^{3+}$. Damaged sites are shown in red. A schematic of the oxidative damage in the rhodium tethered, double guanine-containing duplex, studied previously, is also shown.

reflecting direct reaction by the rhodium complex, damage is observed only at the end of the duplex, as expected for our covalently tethered photooxidant. Importantly, this establishes the duplex end as the site of radical injection. Furthermore, the observation of direct strand scission ensures duplex formation, as discussed earlier. After irradiation of **DQ-2** and **DQ-3** at 365 nm, damage is observed at guanines in the quadruplex portion. As we had observed with **DQ-1**, for all of the 5′-GGG-3′ triple guanine sites comprising the quadruplex regions, damage is observed almost exclusively at the 3′- and 5′-Gs; there is little damage at the center guanine of each triplet. It is noteworthy that little damage is observed in the duplex region, which includes a guanine doublet site. Histograms of the oxidative damage observed after 120 min of irradiation at 365 nm for **DQ-2** and **DQ-3** are shown in Figure 6B. Because of poor resolution on the gel as compared to other triple guanine sites, the 5′-GGG-3′ at the 3′-end of the sequence appears as only two peaks in the histogram; these two peaks correspond to the 3′ and 5′-Gs.

Schematics summarizing the CT damage in the duplex/quadruplex conjugates as well as in the rhodium-tethered assembly containing the same duplex sequence studied previously (*19*) are shown in Figure 7 (oxidatively damaged sites are in red). The duplex assembly was damaged at both 5′-Gs of the 5′-GG-3′ guanine doublets. In all three duplex/quadruplex conjugates, irrespective of rhodium binding site or presence of a guanine doublet, the two outer tetrads are oxidatively damaged while the center guanines of the 5′-GGG-3′ guanine triplets, which form the center tetrad, are not damaged; little significant damage occurs within the duplex region of the duplex/quadruplex conjugates.

DISCUSSION

To explore CT in a DNA structure proposed to be biologically important for oxidative damage, DNA conjugates containing adjacent duplex and guanine quadruplex regions were designed. Circular dichroism is a valuable tool for monitoring the formation of antiparallel guanine quadruplex structures in solution due to distinctive signals at 260 and 290 nm. In combination with a DMS protection assay, native gel electrophoresis, and high energy irradiation of the rhodium photooxidant, we were able to characterize the formation of both the duplex and the quadruplex regions of the conjugate assemblies. The melting temperature studies provide a measure of stability of the DNA conjugates; with melting temperatures of ~60 °C, these assemblies are quite robust.

In assemblies containing a tethered photooxidant, radical injection occurs in the duplex region and must be funneled to the quadruplex region to yield damage. Irradiation at 313 nm marks the site of rhodium binding through direct strand scission, and under the conditions utilized for CT experiments, this direct strand cleavage occurs exclusively within the duplex region; only at much higher concentrations is some cleavage detectable within the quadruplex. Thus, at the concentrations utilized, CT to yield damage within the quadruplex must originate within the duplex region. The reaction is therefore within an individual assembly and does not involve interassembly interactions. Native gel electrophoresis also supports this intra-assembly reaction, in that no evidence of aggregation or multimer formation is detected.

The schematics in Figure 1 illustrate the base stack of the duplexes aligning with the stacked tetrads of the quadruplexes. This alignment was originally unanticipated and required experimental support. In fact, molecular modeling of a DNA conjugate containing the same 22 base quadruplex forming overhang and dT_{12}:dA_{12} as the duplex sequence revealed very little base−base overlap between the duplex and the folded quadruplex regions (*37*). In this scenario, CT from a duplex-bound photooxidant to the bases of the quadruplex would not be possible since a continual array of π-orbitals is requisite. CT in DNA is exquisitely sensitive to base stacking and dynamics; insertion of a π-stacking perturbation such as a base bulge, mismatch, or nonaromatic moiety can turn off CT (*38*−*40*). The observation of CT to the quadruplexes of the conjugates designed here indicates that sufficient base−base overlap does exist at the duplex/quadruplex junction. We also explored CT in conjugates containing a three base 5′-ATA-3′ linker between the duplex and the quadruplex regions (Supporting Information). The amount of oxidative damage in the quadruplex regions of these conjugates was very small, suggesting that a linker region provides too much flexibility at the duplex/quadruplex junction, resulting in poor base stacking overlap and therefore inefficient CT. In the absence of the linker, however, sufficient interactions between the two regions provide a route for CT. Indeed, in all three conjugates examined, similar damage patterns are obtained, suggesting that the guanine quadruplex serves as the trap for the oxidizing equivalents, regardless of the site of radical injection. Hence, in these assemblies, it is clear that radicals generated in the duplex/quadruplex conjugate are preferentially trapped in the folded quadruplex. If instead, deeper traps were to exist within the duplex region, possibly they would provide effective competition for damage.

The pattern of damage within the quadruplex is also easily distinguished from that for a 5′-GGG-3′ triplet within duplex DNA. One explanation for the damage pattern observed, specifically, the lack of damage at the center tetrad, is that the stacking overlap of guanines in a quadruplex results in lowered oxidation potentials for the 5′- and 3′-guanines. Stacking of guanines in double helical DNA has been shown, both experimentally and theoretically, to lead to lowered oxidation potentials. For instance, 6-31G* single-point calculations predict the ionization potential for a single nonstacked guanine base to be 7.75 eV, while that of a guanine doublet, triplet, and quadruplet in duplex DNA is predicted to be 7.28, 7.07, and 6.98 eV, respectively (*41*, *42*). Furthermore, similar calculations predict that the HOMO of these guanine sequences stacked as in a duplex are localized on the 5′-G. Previous experiments demonstrated that after photoactivation of an intercalating oxidant, oxidative damage is observed exclusively at the 5′-G of 5′-GG-3′ guanine doublets (*30*).

To ascertain if the stacking of the bases in the quadruplex results in varying oxidation potentials for the guanines, 6-31G* single-point calculations analogous to those performed on the stacked bases of duplex DNA were performed. Preliminary calculations on the stacked guanines arranged in the geometry of an antiparallel quadruplex do not indicate a higher oxidation potential for the guanines comprising the center tetrad. This is consistent with experimental work reported by Thorp and Szalai (*25*). Using electrochemical generation of a $Ru(bpy)_3^{3+}$ oxidant to test for competitive damage based on oxidation potential, only minor differences in the amount of oxidation of an oligonucleotide in the duplex versus quadruplex form were observed. This is in contrast to a 12-fold difference in guanine oxidation for an oligonucleotide containing single Gs versus 5′-GG-3′ guanine doublets.

If the pattern of damage within the guanine triplets of the quadruplex structure does not reflect a variation in oxidation potential based upon guanine stacking, a more likely explanation for the oxidative damage pattern observed relates to differential trapping of the guanine radical. It has been established that long-range CT results in the formation of guanine cation and neutral radicals that then react irreversibly with H_2O and O_2 to form oxidative products that include 8-oxo-guanine, formamidopyrimidine, oxazalone, and imidazalone derivates visualized by gel electrophoresis (*43*). Access to diffusible molecular oxygen may be limited in the core of the quadruplex leading to a decreased efficiency of radical trapping at the center tetrad. This reduced access would lead to the damage pattern we observe.

These quadruplex structures may be physiologically relevant with respect to oxidative damage within the cell. Recently, Hurley and co-workers have shown in vivo that the purine-rich strand of the nuclease hypersensitivity element III_1 can form intramolecular guanine quadruplexes; the addition of a quadruplex-stabilizing cationic porphyrin stabilizes the quadruplex, which in turn serves as a transcriptional repressor element (*6*). These quadruplex structures may also exist at telomeres, although obtaining in vivo evidence has been more elusive. Intriguingly, the results provided here suggest that DNA quadruplexes could, in fact,

serve as traps of oxidative damage in the genome. Since trapping of charges at the guanine doublet of the duplex region, a known thermodynamic trap of electronic holes in DNA, was not found to be competitive with trapping within the folded quadruplex, the quadruplexes must provide a more effective trap.

Finally, the results obtained in this work may also aid in elucidating the DNA sequences that form guanine quadruplexes in vivo. The 5′-GGG-3′ guanine triplets composing the guanine quadruplexes show an oxidative damage pattern of 5′-G ∼ 3′-G ≫ center-G after CT from a rhodium photooxidant. In contrast, the oxidative damage pattern observed at 5′-GGG-3′ guanine triplets in duplex DNA packaged within nuclei after incubation and photoactivation of a rhodium intercalator is 5′-G > center-G > 3′-G (*23*); this is the damage pattern typically observed after long-range CT in duplex DNA. Therefore, by observing CT damage patterns in different regions of the genome, one may be able to distinguish purine rich sequences that in vivo form quadruplex structures. Hence, studies of long-range oxidative DNA damage in vivo by CT may provide a tool to assess quadruplex formation.

SUPPORTING INFORMATION AVAILABLE

Methylation protection results for **DQ-1** and **DQ-2**, native gel electrophoresis of duplex/quadruplex conjugates, melting temperature studies of quadruplex forming strand and duplex alone, and CT damage in the duplex/quadruplex conjugate containing an ATA linker. This material is available free of charge via the Internet at http://pubs.acs.org.

REFERENCES

1. Mergny, J. L., and Helene, C. (1998) *Nat. Med. 12*, 1366.
2. Parkinson, G. N., Lee, M. P. H., and Neidle, S. (2002) *Nature 417*, 876.
3. Neidle, S., and Read, M. A. (2001) *Biopolymers 56*, 209.
4. Patel, D. J., Bouaziz, S., Kettani, A., and Wang, Y. (1999) in *Oxford Handbook of Nucleic Acid Structure* (Neidle, S., Ed.) pp 398, Oxford University Press, Oxford.
5. Rezler, E. M., Bearss, D. J., and Hurley, L. H. (2003) *Annu. Rev. Pharm. Tox. 43*, 359.
6. Siddiqui-Jain, A., Grand, C. L., Bearss, D. J., and Hurley, L. H. (2002) *Proc. Natl. Acad. Sci. U.S.A. 99*, 11593.
7. Williamson, J. R., Raghuraman, M. K., and Cech, T. R. (1989) *Cell 59*, 871.
8. Miura, T., and Thomas, G. J., Jr. (1994) *Biochemistry 33*, 7848.
9. Hardin, C. C., Henderson, E., Watson, T., and Prosser, J. K. (1991) *Biochemistry 30*, 4460.
10. Gilbert, D. E., and Feigon, J. (1999) *Curr. Opin. Struct. Biol. 9*, 305.
11. Blackburn, E. H. (1991) *Nature 350*, 569.
12. Collins, K. (2000) *Curr. Opin. Cell Biol. 12*, 378.
13. Wright, W. E., Tesmer, V. M., Huffman, K. E., Levene, S. D., and Shay, J. W. (1997) *Genes Dev. 11*, 2801.
14. von Zglinicki, T. (2002) *Trends Biochem. Sci. 27*, 339.
15. Núñez, M. E., and Barton, J. K. (2000) *Curr. Opin. Chem. Biol. 4*, 199.
16. Schuster, G. B. (2000) *Acc. Chem. Res. 33*, 253.
17. Giese, B. (2002) *Annu. Rev. Biochem. 71*, 51.
18. Lewis, F. D., Letsinger, R. L., and Wasielewski, M. R. (2001) *Acc. Chem. Res. 34*, 159.
19. Núñez, M. E., Hall, D. B., and Barton, J. K. (1999) *Chem. Biol. 6*, 85.
20. Ly, D., Sanii, L., and Schuster, G. B. (1999) *J. Am. Chem. Soc. 121*, 9400.
21. Nuñez, M. E., Noyes, K. T., Gianolio, D., McLaughlin, L. W., and Barton, J. K. (2000) *Biochemistry 39*, 6190.
22. Nuñez, M. E., Noyes, K. T., and Barton, J. K. (2002) *Chem. Biol. 9*, 403.
23. Nuñez, M. E., Holmquist, G. P., and Barton, J. K. (2001) *Biochemistry 40*, 12465.
24. Friedman, K. A., and Heller, A. (2001) *J. Phys. Chem. B 105*, 11859.
25. Szalai, V. A., and Thorp, H. H. (2000) *J. Am. Chem. Soc. 122*, 4524.
26. Beaucage, S. L., and Caruthers, M. H. (1981) *Tetrahedron Lett. 23*, 1859.
27. Warshaw, M. M., and Tinoco, I., Jr. (1966) *J. Mol. Biol. 20*, 29.
28. Holmlin, R. E., Dandliker, P. J., and Barton, J. K. (1999) *Bioconj. Chem. 10*, 1122.
29. Sitlani, A., Long, E. C., Pyle, A. M., and Barton, J. K. (1992) *J. Am. Chem. Soc. 114*, 2303.
30. Hall, D. B., Holmlin, R. E., and Barton, J. K. (1996) *Nature 382*, 731.
31. Parkinson, G. N., Lee, M. P. H., and Neidle, S. (2002) *Nature 417*, 876.
32. Wang, Y., and Patel, D. J. (1993) *Curr. Biol. 1*, 263.
33. Balagurumoorthy, P., and Brahmachari, S. K. (1994) *J. Biol. Chem. 269*, 21858.
34. Lu, M., Gao, Q., and Kallenbach, N. R. (1993) *Biochemistry 32*, 598.
35. Dapic, V., Abdomerovi, V., Marrington, R., Peberdy, J., Rodger, A., Trent, J. O., and Bates, P. J. (2003) *Nuc. Acids Res. 31*, 2097−2107.
36. Risitano, A., and Fox, K. R. (2003) *Biochemistry 42*, 6507.
37. Ren, J., Qu, X., Trent, R. O., and Chaires, J. B. (2002) *Nucleic Acids Res. 30*, 2307.
38. Hall, D. B., and Barton, J. K. (1997) *J. Am. Chem. Soc. 119*, 5045.
39. Bhattacharya, P. K., and Barton, J. K. (2001) *J. Am. Chem. Soc. 123*, 8649.
40. Rajski, S. R., and Barton, J. K. (2001) *Biochemistry 40*, 5556.
41. Saito, I., Takayama, M., Sugiyama, H., Nakatani, K., Tsuchida, A., and Yamamoto, M. (1995) *J. Am. Chem. Soc. 117*, 6406.
42. Prat, F., Houk, K. N., and Foote, C. S. (1998) *J. Am. Chem. Soc. 120*, 845.
43. Burrows, C. J., and Muller, J. G. (1998) *Chem. Rev. 98*, 1109.

BI0351965